Hydrobiologia (2016) 780:5–20
DOI 10.1007/s10750-015-2584-7

EUROPEAN LARGE LAKES IV

Semi-analytical prediction of Secchi depth using remote-sensing reflectance for lakes with a wide range of turbidity

Takehiko Fukushima · Bunkei Matsushita · Yoichi Oyama · Kazuya Yoshimura · Wei Yang · Meylin Terrel · Shimako Kawamura · Akito Takegahara

Received: 6 September 2015 / Revised: 3 November 2015 / Accepted: 6 November 2015 / Published online: 28 December 2015

Abstract It is crucial to monitor light environments in large lakes using satellite remote-sensing data. Many studies have proposed prediction schemes of transparency information, but most of them were site-specific. Here, we applied semi-analytical retrieval procedures of inherent optical properties from in situ-measured remote-sensing reflectance and then predicted the Secchi depth (SD) using contrast transmittance theory. Two types of water regions (clear or turbid waterbodies) were first classified based on spectral characteristics, and a selection from two retrieval procedures for clear and turbid water bodies was made. The relationship between the SD and the sum of attenuation coefficients (beam and diffuse attenuation coefficients), which arises in contrast transmittance theory, was determined by analyzing the data from the previous research. The predicted SD values were compared with the observed values in 10 Japanese lakes with a wide variety of turbidity (SD 0.4–17 m). Fairly good agreement between the predicted and observed SD values was obtained, indicating the usefulness of this prediction scheme. We then made an accuracy comparison with the results obtained by previous studies, and we discuss the coefficients and the discrepancies between the measured and predicted SD values in addition to the future directions of this approach.

Keywords Secchi depth · Lakes · Remote sensing · Semi-analytical prediction · Hybrid model

Guest editors: Paula Kankaala, Tiina Nõges, Martti Rask, Dietmar Straile & Arkady Yu. Terzhevik / European Large Lakes IV. Ecosystem Services and Management in a Changing World

T. Fukushima (✉) · B. Matsushita · M. Terrel · S. Kawamura · A. Takegahara
Graduate School of Life and Environmental Studies, University of Tsukuba, 1-1-1, Tennoudai, Tsukuba, Ibaraki 305-8572, Japan
e-mail: fukushima.takehik.fu@u.tsukuba.ac.jp

Y. Oyama
Marimo Research Center, Kushiro Board of Education, Kushiro, Japan

K. Yoshimura
Sector of Fukushima Research and Development, Japan Atomic Energy Agency, Tokaimura, Japan

W. Yang
Department of Environmental Geochemical Cycle Research, Japan Agency for Marine-Earth Science and Technology, Yokosuka, Japan

W. Yang
State Key Laboratory of Earth Surface Processes and Resource Ecology, Beijing Normal University, Beijing, China

Introduction

Assessing the water clarity of waterbodies is a key issue for environmental monitoring and management. The Secchi depth (SD) is an optical measure of water clarity by human vision and it is determined by all optically active substances (OASs) in the water, i.e., phytoplankton (represented by chlorophyll-*a*), tripton [non-planktonic suspended solids (SSs): Tr], colored dissolved organic matter, and pure water (Mancino et al., 2009). Despite the ease with which SD data can be obtained, the collection of these data frequently and for huge numbers or for large waterbodies is costly and challenging for monitoring agencies (Nelson et al., 2003). Remote sensing offers several advantages such as spatially and temporally extensive coverage and the possibility of measuring many waterbodies simultaneously (Koponen et al., 2002). Therefore, a combination of remote-sensing techniques with precise knowledge on water optics could provide an efficient method to monitor waterbodies.

Many research groups have investigated the relationships between in situ measurements of SD and the spectral response of satellite sensors such as Landsat (Lathrop et al., 1991; Giardino et al., 2001; Kloiber et al., 2002; Nelson et al., 2003; Sawaya et al., 2003; Chipman et al., 2004; Hellweger et al., 2004; Alparslan et al., 2007; Sass et al., 2007; Olmanson et al., 2008; Kabbara et al., 2008; Mancino et al., 2009; Hicks et al., 2013; Olmanson et al., 2014), MODIS (Härmä et al., 2001; Wu et al., 2008), SeaWiFS (Kratzer et al., 2003; Binding et al., 2007), and MERIS (Härmä et al., 2001; Koponen et al., 2002; Kratzer et al., 2008; Giardino et al., 2010). However, most of these studies focused principally on empirical approaches, and thus the final applications tended to be time- and site-specific. For example, if an algorithm has been developed for an algae-dominant water body, it is difficult or impossible to apply this algorithm to a non-algae-dominant water body, because different OASs in the water bodies will result in different bands selection and thus different algorithms. Thus, for example, the SD prediction scheme through chlorophyll-*a* (Chl-*a*) possibly results in fairly large estimation errors.

In parallel, substantial efforts have been made to retrieve the inherent optical properties (IOPs) of waterbodies from spectral measurement of water color. These efforts have included an empirical algorithm (Lee et al., 1998), a spectral optimization approach (Roesler & Perry, 1995), an artificial neural network (Doerffer & Schiller, 2007), a linear matrix inversion method (Hoge & Lyon, 1996), and a quasi-analytical algorithm (QAA; Lee et al., 2002). Among these approaches, the QAA, which is an inversion based on the semi-analytical relationship between remote-sensing reflectance and the IOPs, is quite effective and simple to implement. Chen et al. (2007) estimated the SD in Tampa Bay, Florida by processing SeaWiFS satellite imaginary based on a two-step process, first estimating the diffuse attenuation coefficient at 490 nm [$K_d(490)$] using this semi-analytical approach, and then the SD using as empirical relationship with $K_d(490)$. This method has provided an excellent estimate of in situ SD values, but its applicability is uncertain for wider SD ranges of waterbodies because of both the empirical relationship used with $K_d(490)$ estimation and the far lesser reliability of the semi-analytical approach for inland waters, particularly turbid and eutrophic waters.

There is another approach—a semi-analytical approach that uses the contrast transmittance theory (Tyler, 1968; Preisendorfer, 1986). In this approach, SD values are expressed using the beam and diffuse attenuation coefficients in the range of visible wavelengths, which could be related to the IOPs (i.e., the absorption and scattering coefficients) of the targeted water. This approach has seldom been used to estimate SDs in lakes because the measurement of attenuation coefficients and/or IOPs requires a high-level of technique and a great deal of labor in the field or laboratory; a similar trial has been done for ocean transparency using MERIS, MODIS, and SeaWiFS data, however, showing substantial prediction errors (Doron et al., 2011). However, it may be possible to use the IOP-retrieving algorithm from remote-sensing reflectance, as mentioned above.

In this approach, IOPs are estimated using remote-sensing reflectance spectra at the first stage, and then the values of SD are predicted using the contrast transmittance theory at the second stage. Because both stages are based on semi-analytical algorithms, this approach is expected to be applicable to wider water regions compared to the method based on empirical relationships. To establish this approach, an algorithm for retrieving IOPs in turbid waters is absolutely necessary.

Yang et al. (2013) proposed a modified algorithm (enhanced QAA for turbid waters: QAA_turbid) to retrieve total absorption and backscattering coefficients based on a semi-analytical estimation model for turbid inland waters and they described the potential of this algorithm to accurately retrieve the IOPs using in situ reflectance spectra. A hybrid scheme could thus be constructed for the estimation of IOPs: original QAA for clear waters and QAA_turbid for turbid waters. However, a classification procedure is necessary for choosing which IOPs estimation method should be applied.

In the present study, we constructed a semi-analytical algorithm for estimating SD value using remote-sensing reflectance spectrum. We then compared the estimated SD values with the measured values that were obtained in 10 Japanese lakes with a wide variety of turbidity. We propose a classification procedure between clear and turbid states and the coefficient in the contrast transmittance theory. Then, an accuracy comparison with the results obtained by previous studies is made. The coefficients used in the proposed system and discrepancies between the measured and predicted SDs are discussed in addition to the future directions for this approach. In this study, we use in situ-measured reflectance spectra in the range of 400–780 nm at 1-nm intervals. The application of the present approach to satellite data is a future challenge.

Methods

In situ data collection

Measurements of SDs and corresponding reflectance spectra, and collections of water samples were done at 10 lakes in Japan (Table 1; Fig. 1) during the years 2009–2014. Fifteen data collection campaigns were used for this study: four campaigns in Lake Kasumigaura, two campaigns in Lakes Biwa and Shoji, and one campaign for the other seven lakes. The numbers of the observation points at the respective campaigns are shown in Table 1.

SDs were measured using a standard white circular panel (0.3 m in dia.). Reflectance measurements were performed between 9:30 and 16:00 h local time. The upwelling radiance (L_u), the downward irradiance (E_d, reflected upwards from the SRT-99-100 Spectralon reflectance panel®), the downward radiance of skylight (L_{sky}), and the upwelling radiance from the reflectance panel shaded from direct sunlight (L_{shade}) were measured at each site using a FieldSpec HandHeld spectroradiometer (Analytical Spectral Devices, Boulder, CO, USA) in the range of 325–1075 nm at 1-nm intervals. "L_{sky}" refers to the diffused radiation of the sky, which contains no information on water properties, and hence must be eliminated. To avoid the influence of reflection and shading from the boat, all spectral observations were measured at the zenith angle of around 58°. In addition, the direction of each spectral observation was 90° to the plane of the sun to avoid the effect of sun glint.

The above-water remote-sensing reflectance (R_{rs}) was calculated approximately using the equation given by Mobley (1999):

$$R_{rs} \approx \left(\frac{L_u}{E_d} - \frac{F(\theta) \cdot L_{sky}}{E_d}\right) \cdot \mathrm{Cal} \cdot 100 \quad (1)$$

where Cal is the spectral reflectance calibration factor for the Spectralon reflectance panel (SRT-99-100). $F(\theta)$ represents the reflectance of the skylight at the air–water interface ranging from 0.022 to 0.025, and θ is the measurement view angle (Mobley, 1999). In this study, a constant value of 0.024 was used for $F(\theta)$.

At in situ measurements, the surface waves and clouds affected the obtained reflectance spectra. We thus removed the campaigns when the influence of waves seemed considerable. The upwelling radiances were measured 10 times, and then the lower five data were averaged to get the value of L_u. Here, we calculated the coefficient of variation (CV; the standard deviation divided by the average) of the lower five radiances averaged in the range of 400–750 nm and considered the influence of waves insignificant if the coefficient was <0.07. All of the campaigns shown in Table 1 satisfied this condition (more than 10 campaigns not shown in Table 1 were unavailable). The influence of waves surely relates to wind velocity; for example, the maximum wind velocities (3.3, 4.5 and 3.9 m/s at Hikone, Nagahama, and Imazu near the lake, respectively) during the excluded campaign in Lake Biwa (6 September 2010) were higher than those during the included campaigns (2.6, 2.2, and 2.0 m/s on 17 August 2009 and 2.2, 2.0, and 2.2 m/s on 12 October 2011 at those stations, respectively) (Japan Meteorological Agency, 2015).

Next, the influence of clouds was considered using the value of L_{shade} divided by (E_d/π). For the

Table 1 The 10 surveyed lakes in Japan and their dimensions, sampling information, and water quality

Lake names	Surface area (km^2)	Maximum depth (m)	Observation dates	Number of points	Range of SD (m)	Chlorophyll-*a* (mg/l)	SS (mg/l)
Biwa	670.3	103.8	17 August 2009	6	3.2–9.2	0.69–1.3	0.57–1.9
			12 October 2011	9	4.2–9.3	1.8–2.9	0.77–2.0
Kasumigaura	167.6	11.9	12 August 2009	3	0.50–0.70	55.4–106	16.2–22.5
			1 September 2009	14	0.40–0.70	39.7–106	16.4–55.7
			17 March 2010	2	0.59–0.60	80.7–82.4	27.5–27.5
			18 May 2010	24	0.50–0.75	37.0–91.7	18.0–30.1
Shirakaba	0.4[a]	9.1[a]	22 July 2010	1	3.5	2.3	2.8
Suwa	12.9	7.6	21 July 2010	10	1.6–1.9	9.8–11.3	4.6–6.1
Ikeda	10.9	233.0	5 September 2011	1	9.3	1.4[c]	0.65[c]
Unagi-ike	1.2	55.8	5 September 2011	1	12.8	0.53[c]	0.39[c]
Akan	13.0	44.8	28 August 2013	1	6.7	0.8	1.5
Motosu	4.7	121.6	11 March 2014	1	16.4	0.57	0.38
Shoji	0.5[b]	15.2[b]	11 March 2014	1	3.5	8.5	2.4
			22 August 2014	1	4.2	3.2	1.7
Sai	2.1	71.7	22 August 2014	2	6.8–7.1	1.8	1.3

[a] Ha et al. (2015)

[b] Wikipedia, other information on lake dimensions: Chronological Scientific Tables

[c] Measured by sensor and estimated with calibration lines

Fig. 1 The location of the 10 lakes in Japan

subsequent calculation, we used the measurement when this value was <0.25. The numbers of measurements that satisfied this condition are shown in Table 1 as the number of points. In addition, the threshold was changed to 0.20 to evaluate the influence of clouds for estimating SDs. The R_{rs} spectra used for the further analysis are shown in Fig. 2.

For the collected water samples, Chl-*a* was extracted using methanol (100%) at 4°C under dark conditions for 24 h. The extract was then centrifuged at 3,000 rpm for 10 min and analyzed spectrophotometrically to estimate the concentration of Chl-*a* according to SCOR-UNESCO equations (1966). The concentrations of the SSs were determined gravimetrically. Samples were filtered through pre-combusted Whatman GF/F filters at 500°C for 4 h to remove the dissolved organic matter in suspension, which was then dried at 105°C for 4 h and weighed to obtain SS. Table 1 provides a summary of the relevant characteristics of the studied waterbodies together with the SDs and OASs (Chl-*a* and SS) concentration ranges obtained from the in situ data collection.

Development of a semi-analytical model for estimating SDs

The flow chart of the following proposed method is shown in Fig. 3.

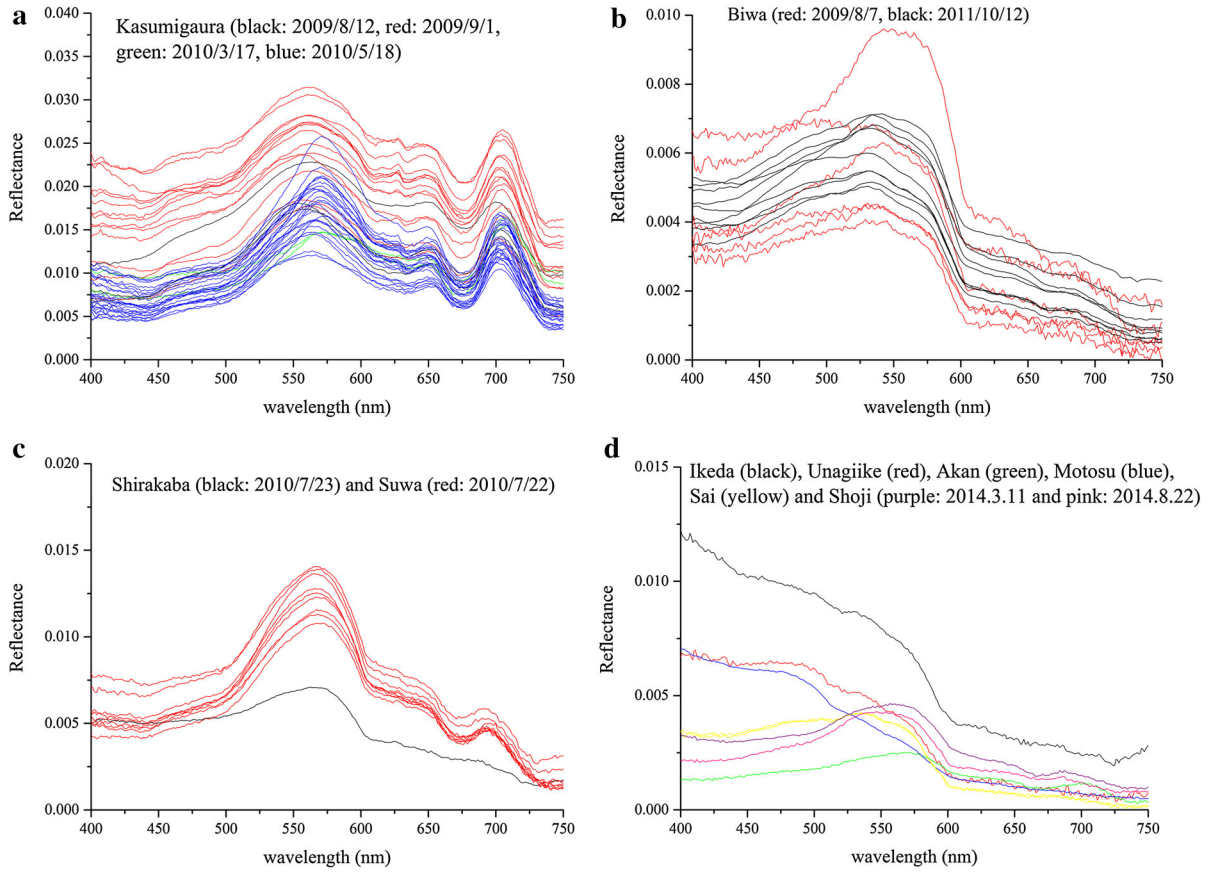

Fig. 2 In situ reflectance spectra used in this study. **a** Lake Kasumigaura, **b** Lake Biwa, **c** Lake Suwa and Lake Shirakaba, **d** other lakes

Stage 1: retrieving IOPs from reflectance spectra

As explained below, two algorithms for retrieving IOPs from reflectance spectra were prepared for clear and turbid waters, respectively. Since a selection between them is therefore necessary, we used the maximum Chl index [MCI: R_{rs}(709 nm) − R_{rs}(681 - nm)], which is a measure of the reflectance peak at 709 nm in water-leaving reflectance. Gower et al. (2005) have demonstrated use of this index to detect plankton blooms. This is because the absorption by Chl reduces radiance at wavelengths shorter than 700 nm, while absorption by water reduces radiance at wavelengths longer than 720 nm, leading to a radiance peak at the wavelength of minimum absorption, near 709 nm. This index was used to select the most appropriate algorithm for estimating Chl-*a* concentrations among a blue–green algorithm, an algorithm with a two-band index, and an algorithm with a three-band index (Matsushita et al., 2015). In this study, three ranges were set for the selection of Chl-*a* estimating algorithms: (1) when the MCI was $\leq$0.0001, then the blue–green algorithm was used, (2) when 0.0001 $<$ MCI $\leq$ 0.0016, then the two-band algorithm was used, and (3) when MCI >0.0016, then the three-band index algorithm was used. The MCI values 0.0001 and 0.0016 approximately corresponded to the Chl-*a* values 10 and 25 mg/m^3, respectively, based on a linear relationship between MCI and Chl-*a* ($R^2 = 0.76$, $P < 0.001$) using the data taken in five Asian lakes. The results showed that this hybrid algorithm performed well in these lakes (Lakes Biwa, Kasumigaura, and Suwa used in this study and Lakes Dianchi and Erhai in China not used in this study but explained in Matsushita et al., 2015).

Following the original proposal of the QAA by Lee et al. (2002), several updates have been presented (Lee et al., 2005, 2007). For clear waters, we used a

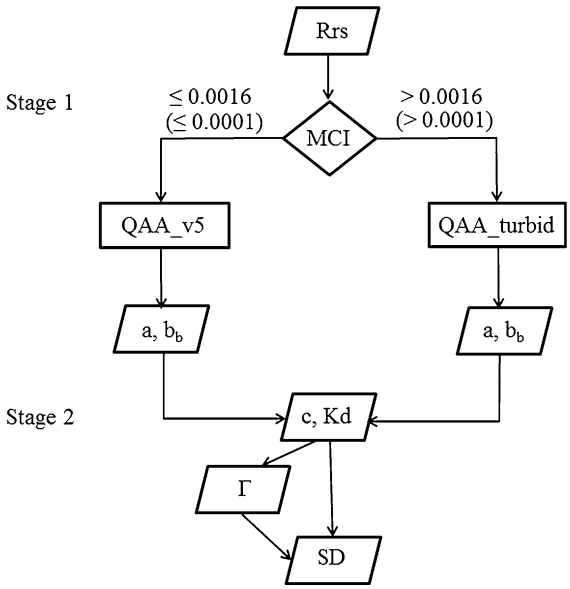

Fig. 3 Flow chart of the semi-analytical prediction of Secchi depth. R_{rs} remote-sensing reflectance, *MCI* maximum chlorophyll index, *QAA_v5* quasi-analytical algorithm version 5, *QAA_turbid* quasi-analytical algorithm for turbid waters, a absorption coefficient, b_b backscattering coefficient, c beam attenuation coefficient, K_d diffuse attenuation coefficient, Γ coupling constant, *SD* Secchi depth

recent version (version 5, denoted QAA_v5 hereafter; Lee et al., 2009) in which four empirical estimation models have been updated compared to previous versions. The flow of QAA_v5 is shown in Table 2, and the steps up to Step 6 were used in this study. There are mainly three limitations that challenge the applicability of QAA_v5 in turbid inland waters. The first limitation regards about the estimation model for total absorption at the reference band (Step 2 in Table 2), which is empirically derived from the synthetic dataset. The second limitation regards the Y estimation model (Step 4), which was calibrated using the data obtained in oceans or coastal areas. The third limitation is the algebraic equations for estimating the phytoplankton absorption (Steps 7 and 8), in which the ratios were empirically determined in a manner similar to that of Step 4. Yang et al. (2013) proposed the enhancement of the QAA for turbid waters in three ways: (1) the extension of the reference wavelength to the near-infrared band, (2) the development of a semi-analytical estimation model for the spectral slope of particle backscattering, and (3) the development of an empirical estimation model for the phytoplankton absorption coefficient at 443 nm. The main steps are shown in Table 3 (denoted "QAA_turbid" hereafter) and the steps up to Step 5 were used in the present study.

Thus, we applied two MCI thresholds for the selection of IOP-retrieving algorithms, i.e., (1) when MCI $\leq$0.0001, then QAA_v5 and (2) when MCI $>$0.0016, then QAA_turbid. In addition, both algorithms were compared in the range of $0.0001 < \mathrm{MCI} \leq 0.0016$.

Stage 2: estimating SDs from IOPs

Based on the constant transmittance theory (Tyler, 1968; Preisendorfer, 1986), the following SD relation was developed.

$$\mathrm{SD} = \frac{\Gamma}{\int_{\lambda_1}^{\lambda_2} \mathrm{Eye}(\lambda) \cdot I_{\mathrm{surface}}(\lambda)[\boldsymbol{c}(\lambda) + \boldsymbol{K}_{\mathrm{d}}(\lambda)]\mathrm{d}\lambda / \int_{\lambda_1}^{\lambda_2} \mathrm{Eye}(\lambda) \cdot I_{\mathrm{surface}}(\lambda)\mathrm{d}\lambda} \quad (2)$$

where $\boldsymbol{c}$ and $\boldsymbol{K}_{\mathrm{d}}$ are depth-averaged (from the water surface to the SD) beam and diffuse attenuation coefficients, respectively. When these coefficients do not change vertically, they are expressed simply as c and K_{d}, respectively. Hereafter, we assume their vertical constancy. $\mathrm{Eye}(\lambda)$ and $I_{\mathrm{surface}}(\lambda)$ are the photopic response of the human eye and the downwelling irradiance at the water surface, respectively, and they are a function of the wavelength: λ. The denominator of Eq. (2) indicates the sum of c and K_{d} weighted toward the wavelength dependency of the photic response and the downwelling irradiance over the range of visible wavelengths from λ_1 to λ_2 (Preisendorfer, 1986). The photopic function possesses a maximum of around 550 nm and near zero at

Table 2 Steps of the quasi-analytical algorithm for retrieving IOPs in clear waters: QAA_v5 (Lee et al., 2009)

Steps	Properties	Derivations	Approaches
Step 0	r_{rs}	$=R_{rs}/(0.52 + 1.7R_{rs})$	Semi-analytical
Step 1	$\mu(\lambda) \equiv \frac{b_b(\lambda)}{a(\lambda)+b_b(\lambda)}$	$= \frac{-0.089+\sqrt{0.089^2+4\times0.125r_{rs}}}{2\times0.125}$	Semi-analytical
Step 2	$a(\lambda_0)$	$= a_w(\lambda_0) + 10^{-1.146-1.366\chi-0.469\chi^2}$	Empirical
		$\chi = \log\left(\frac{r_{rs}(443)+r_{rs}(490)}{r_{rs}(\lambda_0)+5\frac{r_{rs}(667)}{r_{rs}(490)}r_{rs}(667)}\right)$	
Step 3	$b_{bp}(\lambda_0)$	$\frac{\mu(\lambda_0)a(\lambda_0)}{1-\mu(\lambda_0)} - b_{b,w}(\lambda_0)$	Analytical
Step 4	Y	$= 2.0\left(1 - 1.2\exp\left(-0.9\frac{r_{rs}(443)}{r_{rs}(\lambda_0)}\right)\right)$	Empirical
Step 5	$b_{bp}(\lambda)$	$= b_{b,p}(\lambda_0)\left(\frac{\lambda_0}{\lambda}\right)^Y$	Semi-analytical
Step 6	$a(\lambda)$	$= \frac{(1-\mu(\lambda))(b_{b,w}(\lambda)+b_{b,p}(\lambda))}{\mu(\lambda)}$	Analytical
Step 7	$\zeta \equiv a_{ph}(411)/a_{ph}(443)$	$= 0.74 + \frac{0.2}{0.8+r_{rs}(443)/r_{rs}(\lambda_0)}$	Empirical
Step 8	$\xi \equiv a_{dg}(411)/a_{dg}(443)$	$=e^{S(443\ -\ 411)}$	Semi-analytical
		$S = 0.015 + \frac{0.002}{0.6+r_{rs}(443)/r_{rs}(\lambda_0)}$	
Step 9	$a_{dg}(443)$	$= \frac{(a(411)-\zeta a(443))-(a_w(411)-\zeta a_w(443))}{\xi-\zeta}$	Analytical
Step 10	$a_{ph}(\lambda)$	$= a(\lambda) - a_w(\lambda) - a_{dg}(443)e^{-S(\lambda-443)}$	Analytical

Table 3 Steps of the quasi-analytical algorithm for retrieving IOPs in turbid waters: QAA_turbid (Yang et al., 2013)

Steps	Properties	Derivations	Approaches
Step 0	r_{rs}	$=R_{rs}/(0.52 + 1.7R_{rs})$	Semi-analytical
Step 1	$\mu(\lambda) \equiv \frac{b_b(\lambda)}{a(\lambda)+b_b(\lambda)}$	$= \frac{-0.089+\sqrt{0.089^2+4\times0.125r_{rs}}}{2\times0.125}$	Semi-analytical
Step 2	$b_{bp}(\lambda_0)$	$= \frac{\mu(\lambda_0)a_w(\lambda_0)}{1-\mu(\lambda_0)} - b_{b,w}(\lambda_0)$	Analytical
Step 3	Y	$=-372.99\beta^2 + 37.286\beta + 0.84$	Semi-analytical
		$\beta = \log[\mu(750)/\mu(780)]$	
Step 4	$b_{bp}(\lambda)$	$= b_{b,p}(\lambda_0)\left(\frac{\lambda_0}{\lambda}\right)^Y$	Semi-analytical
Step 5	$a(\lambda)$	$= \frac{(1-\mu(\lambda))(b_{b,w}(\lambda)+b_{b,p}(\lambda))}{\mu(\lambda)}$	Analytical
Step 6	$a_{ph}(443)$	$=-0.7488a(411) + 1.392a(443) - a_w(443)$	Empirical

the two ends λ_1 and λ_2 (Takami, 2011), as shown in Fig. 4a. In this study, λ_1 and λ_2 were set at 400 and 750 nm, respectively. We used the smoothed "global tilt" (reference solar spectral irradiance: ASTM G-173) as the downwelling irradiance at the water surface as shown in Fig. 4a.

In addition, Γ is a coupling constant that depends on variations in ambient conditions during measurements (Preisendorfer, 1986). In the present study, the value of Γ was set at (1) 9.7 in all lakes (hereafter indicated as Case 1), (2) 9.7 in turbid lakes and 8.2 in clear lakes (indicated as Case 2), and (3) using the following Eq. (3) (indicated as Case 3, but as Case 4 when using the threshold of cloud influence $[L_{shade}/(E_d/\pi)) = 0.20]$.

$$\Gamma = 8.12 \times \left(\int_{\lambda_1}^{\lambda_2} \mathrm{Eye}(\lambda)\cdot I_{surface}(\lambda)[c(\lambda) + K_d(\lambda)]\mathrm{d}\lambda \Big/ \int_{\lambda_1}^{\lambda_2} \mathrm{Eye}(\lambda)\cdot I_{surface}(\lambda)\mathrm{d}\lambda\right)^{0.1076} \quad (3)$$

The values of (1) and (2) were obtained by the statistical analysis in Terrel et al. (2012). Equation (3) was deduced from the regression analysis between SD

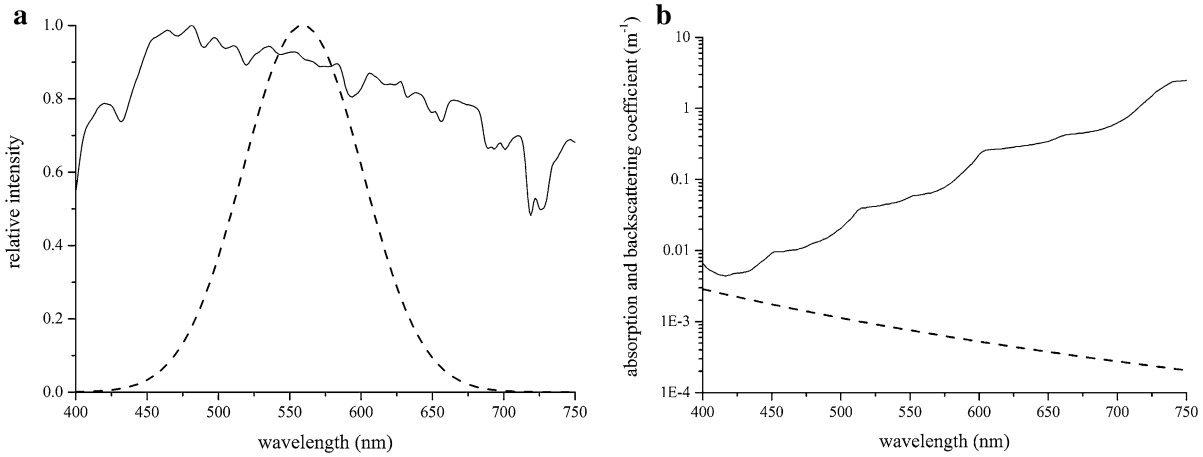

Fig. 4 Optical properties used in this study. **a** The photopic response of the human eye (*broken line*) and the downwelling irradiance at the water surface (*solid line*). **b** The absorption coefficient (*solid line*) and backscattering coefficient of pure water (*broken line*)

and $(c + K_d)$ (Fig. 5) using the data from Davies-Colley (1988) (eight lakes with the range of SD from 0.42 to 17.7 m). Davies-Colley considered that this type of tendency resulted from the change in the angle subtended by the target disk at the eye with SD.

The beam attenuation coefficient $c(\lambda)$ is expressed as the sum of the absorption and scattering coefficients:

$$c(\lambda) = a(\lambda) + b(\lambda) \tag{4}$$

Absorption $a(\lambda)$ and scattering $b(\lambda)$ are IOPs, and thus can be expressed as the sum of the contributions, e.g., pure water, phytoplankton, tripton, and colored dissolved organic matter.

The diffuse attenuation coefficient $K_d(\lambda)$ is estimated based on the relationship given by Kirk (1984):

$$K_d(\lambda) = \left[a(\lambda)^2 + k_\mu \cdot a(\lambda) \cdot b(\lambda)\right]^{0.5} / \mu_0 \tag{5}$$

The coefficient k_μ was estimated from the following equation (Bowers et al., 2000):

$$k_\mu = 0.425 \cdot \mu_0 - 0.19 \tag{6}$$

where μ_0 is the cosine of the zenith angle of refracted solar photons, calculated from the solar zenith angle (SZA) using Snell's law with the appropriate index of refraction for water and air. The SZA was calculated by feeding the date, time, and latitude into the algorithm provided by Nakagawa (2015). In addition, Stage 1 gives the value of backscattering of particles: b_{bp}, and then we used the following equation for calculating the value of b:

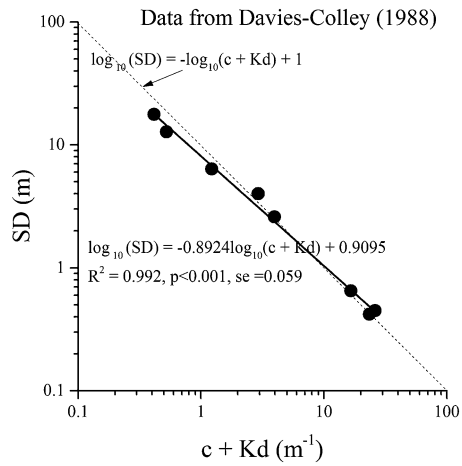

Fig. 5 Relationship between $(c + K_d)$ and SD using the data by Davies-Colley (1988). *Solid line* the regression line. *Dotted line* the line of the negative first power of $(c + K_d)$

$$b = b_{bp} \times \text{coef}_{bp} + b_{bw} \times \text{coef}_w \tag{7}$$

where b_{bw} is backscattering by pure water (Morel, 1974) as shown in Fig. 4b. In the present study, coef_{bp} was set at 55.6 based on the results of the studies such as Mobley et al. (1993) and coef_w was set at 2 due to isotropic scattering. When checking the performance of the present method, we used the absorption coefficient of pure water as shown in Fig. 4b (a_w: Pope & Fry, 1997 from 400 to 700 nm and Hale & Querry, 1973 above 700 nm) as the value of a and considered $b_{bp} = 0$. Then, the SD of pure water was calculated to be 34.8 m.

Accuracy assessment

We used the root-mean-square error (RMSE), the mean normalized bias (MNB), and the normalized RMSE (NRMS) to assess the model performance, defined as follows:

$$\mathrm{RMSE} = \sqrt{\frac{\sum_{i=1}^{N} \left(X_{\mathrm{pred,i}} - X_{\mathrm{meas,i}}\right)^2}{N}} \quad (8)$$

$$\mathrm{MNB}\ (\%) = \bar{\varepsilon} = \frac{\sum_{i=1}^{N} \varepsilon_i}{N} \quad (9)$$

$$\mathrm{NRMS}\ (\%) = \sqrt{\frac{\sum_{i=1}^{N} \left(\varepsilon_i - \bar{\varepsilon}\right)^2}{N}} \quad (10)$$

where $X_{\mathrm{pred,i}}$ and $X_{\mathrm{meas,i}}$ are the predicted and measured values, respectively, N is the number of measurements, and $\varepsilon_i\ (\%) = 100 \cdot \frac{(X_{\mathrm{pred,i}} - X_{\mathrm{meas,i}})}{X_{\mathrm{meas,i}}}$ is the percent difference between the predicted and measured values. The RMSE values depend on the range of SD; in contrast, MNB and NRMS are independent of it, indicating appropriate indicators for evaluating the prediction model in a wide variety of lake light conditions. The standard error (se) of the regression equation (independent variable: measured, dependent variable: predicted) could be calculated as RMSE $\times$ $((N-2)/N)^{0.5}$. When comparing the errors in a logarithmic form, we did not calculate MNB and NRMS. This is because the values of ε_i in a logarithmic form are meaningless.

Results

The comparison between measured and predicted SDs is summarized in Fig. 6 and Table 4. In order to evaluate the influences of the value of Γ and cloud on prediction accuracy, Cases 1–4 are classified based on these values as explained in "Methods" section. In addition, Cases 4-1 and 4-2 are the special cases which used QAA_v5 and QAA_turbid for all lakes, respectively, and Case 4-3 is corresponding to Case 4 but accessed after logarithmically transformed. The threshold MCI is 0.0016 for all cases. In regards to the value of Γ, better results were obtained by changing it with the range of SDs (Case 2: Fig. 6b and Case 3: Fig. 6c) compared to the constant Γ model (Case 1: Fig. 6a). When we set $\Gamma = 8.2$ and 9.7, the values $R^2 = 0.925$ and 0.925, $P < 0.001$ and <0.001, RMSE = 1.20 and 1.53 m, MNB = −22.0 and −14.4%, and NRMS = 37.5 and 41.1% were obtained, respectively, indicating worse agreements (figures not shown). In the comparison of the two changing Γ models, Case 3 gave better agreement than Case 2.

When we removed seven data obtained in bad light-measurement (by cloud) conditions (Case 4: Fig. 6d), the R^2 ($P < 0.001$) and RMSE were worse, but the MNB and NRMS were better compared to the original dataset (Case 3). The removal of the largely underestimated data in this bad cloud conditions (0.55/0.31, 0.65/0.24, 0.50/0.35, 0.50/0.32, 0.58/0.29, 0.60/0.27 m, except one overestimation 0.70/0.89 m; measured SD/predicted SD) resulted in improvement of MNB and NRMS.

In all cases from Cases 1 to 4, the values of MNB were negative, which indicated underestimation on the whole. When we separated the results into the group with SD >1 m and the group ≤1 m using the conditions of Case 4, the former showed overestimation ($R^2 = 0.838$, $P < 0.001$, RMSE = 1.62 m, MNB = 17.0%, NRMS = 34.3%, and $N = 34$), while the latter indicated underestimation ($R^2 = 0.390$, $P < 0.001$, RMSE = 0.20 m, MNB = − 27.7%, NRMS = 28.3%, and $N = 36$ as shown in Fig. 6e). In addition, the evaluation in a logarithmic transformation form gave a higher R^2 value ($P < 0.001$; Case 4-3).

All of the cases shown above used hybrid prediction algorithms with the MCI threshold = 0.0016 (when MCI ≤0.016, then QAA_v5 was used, and when MCI >0.0016, then QAA_turbid was used). We compared the cases with two individual algorithms for retrieving IOPs for clear or turbid waters against all lakes. Both individual algorithms gave worse results (Case 4-1: Fig. 7a only the Lake Kasumigaura data shown by the clear water algorithm and Case 4-2: Fig. 7b by the turbid water algorithm). In particular, the turbid water algorithm sometimes gave quite improbable SDs.

When we changed the threshold MCI to 0.0001, the selection of the retrieving algorithms was altered for nine data (eight for Lake Suwa and one for Lake Akan). The changes in the results were slightly worse ($R^2 = 0.915$, $P < 0.001$, RMSE = 1.18 m, MNB = −12.9%, NRMS = 31.1%), but not so large compared to the results of threshold MCI = 0.0016.

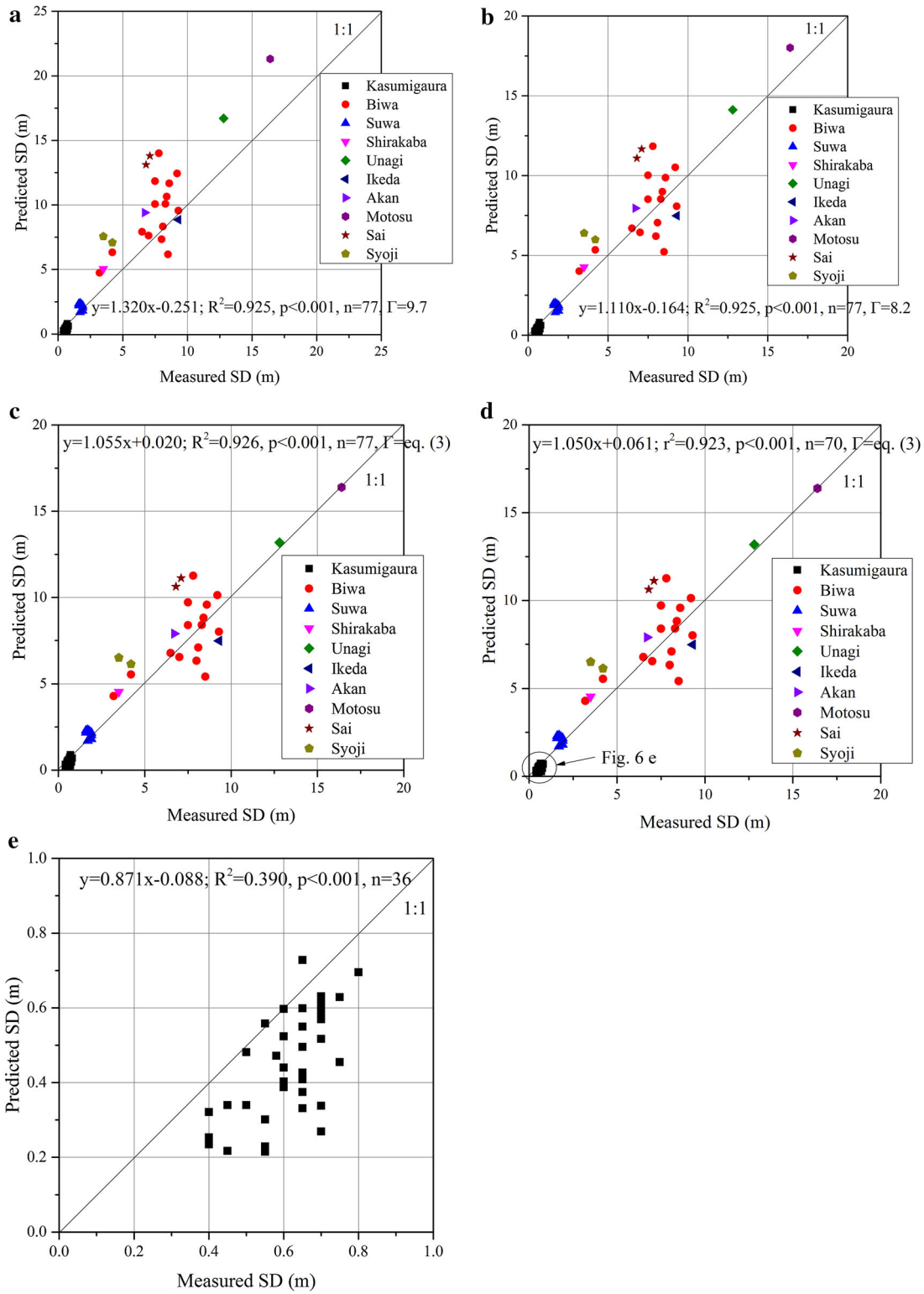

Fig. 6 Measured SDs versus predicted SDs. **a** Case 1 in Table 4, **b** Case 2, **c** Case 3, **d** Case 4, and **e** lakes with SD <1 m (i.e., Lake Kasumigaura) in Case 4 [magnifying the data shown in the *circle* in (**d**)]

Table 4 Summary of the accuracy assessment for predicting SDs

	Case 1	Case 2	Case 3	Case 4	Case 4-1	Case 4-2	Case 4-3
Γ	$\Gamma = 9.7$ in all lakes	$\Gamma = 9.7$ in turbid lakes and $\Gamma = 8.2$ in clear lakes	Equation (3)	Equation (3)	Equation (3)	Equation (3)	Equation (3)
$L_{cloud}/(E_d/\pi)$	<0.25	<0.25	<0.25	<0.20	<0.20	<0.20	<0.20
R^{2*1}	0.925	0.925	0.926	0.923	0.920	0.063	0.957
RMSE (m)	1.88	1.20	1.09	1.14	1.21	10.3	(se = 0.37)
MNB (%)	−7.8	−16.9	−8.7	−6.0	58.0	−14.5	
NRMS (%)	44.3	34.7	32.2	31.4	81.4	146.8	
n	77	77	77	70	70	70	70

Cases 1–3 are classified based on the use of Γ values shown in this table. Case 4 uses the same equation for Γ as Case 3, but different thresholds for cloud influence as described by $(L_{shade}/(E_d/\pi))$. Cases 4-1 and 4-2 are the special cases which use QAA_v5 and QAA_turbid for all lakes, respectively, and Case 4-3 is corresponding to Case 4 but accessed after logarithmically transformed. The classification of clear: MCI $\leqq$0.0016 and turbid: MCI >0.0016 is used for all cases

*1 $P < 0.001$ except for Case 4-2 ($P = 0.036$)

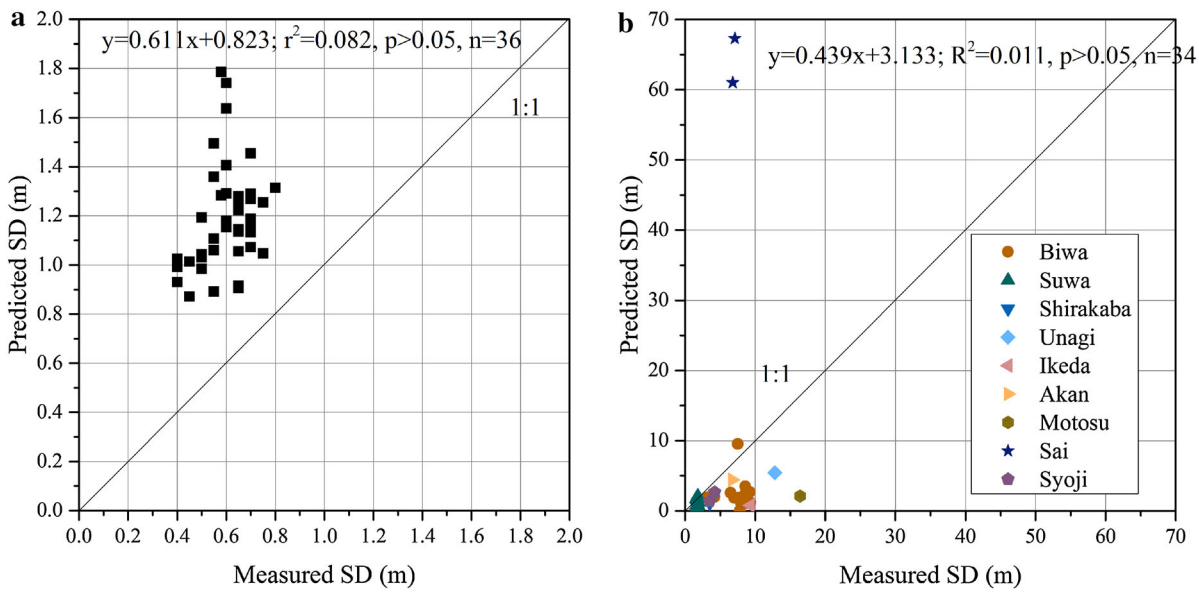

Fig. 7 Measured SDs versus predicted SDs. **a** Lake Kasumigaura by the algorithm for clear waters and Eq. (3) corresponding to Fig. 6e by the algorithm for turbid water. **b** Lakes other than Lake Kasumigaura by the algorithm for turbid water and Eq. (3) corresponding to Fig. 6d by the algorithm for clear water

Discussion

Comparison with previous SD prediction research

To evaluate the prediction accuracy of our approach, we compared our results with those of nine previous results published in seven papers (Table 5). Härmä et al. (2001) used satellite data simulated based on airborne measurements. Lakes were targeted except Tampa Bay (Chen et al., 2007) and Himmerfjärden, a fjord-like bay (Kratzer et al., 2008). Values of se or RMSE were shown for accuracy assessment except Binding et al. (2007) and Kratzer et al. (2008). Our results have higher regression coefficients (Cases 1–4 in Table 4) and a similar level of se (Case 4-3 in Table 4) compared to those studies, although the studies cited in Table 5 used space-born reflectance data containing atmospheric disturbances except Härmä et al. (2001).

Table 5 Examples of accuracy assessment for predicting SDs in previous studies

	Härmä et al. (2001)*1		Chen et al. (2007)*2	Binding et al. (2007)	Olmanson et al. (2008)	Kratzer et al. (2008)*2	Wu et al. (2008)		Hicks et al. (2013)
Sensor	MERIS	MODIS	SeaWiFS	SeaWiFS	Landsat TM and ETM+	MERIS	Landsat TM	MODIS	Landsat ETM+
Regression	Direct	Direct	Direct	Direct	Ln type, each day, 37 days	Ln type	Ln type	Ln type	Ln type
R^2*3	0.84	0.83	0.67	0.72	0.83 (0.71–0.96)	0.79	0.83	0.88	0.67
se	RMSE = 0.7 m	RMSE = 0.6 m	0.55 m		0.29 (0.14–0.41)		0.2	0.37	RMSE = 0.33
N	85		80	306	97 (16–278)	54	25	71	32
SD range	(0.2–7 m)		(0.9–8.0 m)	(0.2–12.5 m)	0.15–14.6 m	(3–7 m)	1.17–2.16 m	0.06–2.84 m	0.05–3.04 m

( ): Reading from the figures in the reference. *1: Simulated satellite data with airborne measurement, *2: coastal waters, *3: $P < 0.001$ for all relationships

The dynamic range (0.4–17 m) of SD estimation in the present study is much greater than those of the previous studies, which were usually done in limited waterbodies with SD values <10 m. Because the models shown in Table 5 are classified as empirical model based on field data, they are so site-specific that an application of the obtained model to other lakes is rather questionable. The determination of the model parameters is a prerequisite for using the models. In contrast, our prediction scheme is almost analytical and therefore probably applicable to any other lakes in the world. In addition, there is no need to determine the model parameters. In this context, our scheme is promising as one of the universal algorithms for SD prediction. The value of Γ, only one parameter, which possibly seems rather empirical, will be discussed below.

In this study, we used in situ reflectance data at the intervals of 1 nm to investigate the possibility of the semi-analytical prediction of SD for lakes with a wide range of turbidity. In the future, it will be necessary to use the reflectance data at limited satellite bands and check the applicability of the IOP-retrieving algorithm to space-born data. The influence of atmospheric correction should be also evaluated in the process of SD prediction.

In the field, we sometimes observe the variability of observed SD due to differences in observer eyesight and/or observation experience. Here, the precision of SD measurement was evaluated based on the field survey in three lakes by 12 individuals. At the same point in these three lakes, each examiner reported his/her observation on SD successively without information on the other examiner's reports. The results showed the following CVs: 13.2% for Lake Sohara (average SD = 3.2 m), 15.1% for Bishamon Pond (average SD = 5.5 m), and 5.6% for Lake Onogawa (average SD = 3.5 m), indicating rather large scatter on SD measurements, due probably to eyesight and/or differences in experience among the examiners. In light of these results, the superiority of SD estimation using reflectance measurement (theoretically zero CV) over direct SD measurement could be expected.

Parameters used in this algorithm

There are many reports about the values of Γ. Tyler (1968) indicated $\Gamma = 8.69$ semi-theoretically based on C_R (the apparent contrast as seen by an observer) = 0.0066 and C_0 (the inherent contrast of a

Secchi disk against its background) = 40. Holmes (1970) reported averaged $\Gamma = 9.42$ using 13 measurements in Goleta Bay, California. Preisendorfer (1986) showed that Γ is related to a psychophysiological parameter of the human eye–brain system, the reflectance of the medium, and the submerged disk reflectance, and he suggested that its reasonable estimates were found at approx. 8–9. Terrel et al. (2012) reported $\Gamma = 10.1$ for Lake Kasumigaura by parameter fitting using long-term data of measured SD and $\Gamma = 9.3$ for the same lake using the limited dataset with an IOP analysis. We used $\Gamma = 9.7$ for all 10 of the lakes as the first trial (Table 4, Case 1), but it gave quite large overestimation values of SDs for the clear lakes. Then, we set $\Gamma = 8.2$ for the clear lakes based on the parameter-fitting result for Lake Biwa (Terrel et al., 2012) similar to the method mentioned above. Nevertheless, $\Gamma = 9.7$ was used for the turbid lakes because underestimated results were mostly seen for the turbid lakes even using $\Gamma = 9.7$. The results showed better agreement (Table 4, Case 2), but a scientific basis for changing Γ is needed.

Holmes (1970) compared SD values with disks of 20-, 30-, or 50-cm dia. and showed its increasing tendency with diameter. However, the statistical significance of SD differences was denied. In contrast, Davies-Colley (1988) indicated a trend of Ψ with clarity. Ψ is defined as z divided by $(c + K_d)$, where z is black-disk visibility (i.e., corresponding to Γ in the case of SD). As the angle subset by the target at the eye decreased with increased range, Ψ apparently also decreased. Davies-Colley gave the equation of Ψ with black-disk visibility. A similar trend is expected for Γ, and thus we determined the relationship as shown in Fig. 5 using the data by Davies-Colley (1988) and then obtained the relation between Γ and $(c + K_d)$ as expressed by Eq. (3). This equation gives $\Gamma = 12.87$ at SD = 0.2 m, $\Gamma = 10.59$ at SD = 1 m, $\Gamma = 9.74$ at SD = 2 m, $\Gamma = 8.01$ at SD = 10 m, and $\Gamma = 7.37$ at SD = 20 m. Since the influence of Γ on SD prediction is considered fairly large for lakes with a wide variety of turbidity, a careful and elaborate measurement on the relationship between Γ and SDs is necessary.

In addition, the maximum SD was calculated to be 34.8 m with the use of the absorption and backscattering coefficients of pure water as mentioned in the "Methods" section. However, for example, Larson et al. (2007) reported the maximum around 41.5 m (June 1997) in Crater Lake, Oregon. Although there is a possibility of champion data obtained by a person with particularly good eyesight, a value of Γ in such a lake and the IOPs should be reexamined together with checks on Eqs. (5)–(7).

Regarding MCI, the data shown in Fig. 7 and Table 4 clearly indicated that the clear and turbid water algorithms should be used for lakes with MCI $\leq$0.0001 and those with MCI >0.0016, respectively. The problem is the selection of the threshold between 0.0001 and 0.0016. A comparison of predicted SDs between the two algorithms is shown in Fig. 8 for Lakes Suwa and Akan. A better agreement was seen for clear water prediction (i.e., using the threshold MCI = 0.0016), but the observed SD is usually between the two values predicted by the clear and turbid water algorithms. The use of the threshold of MCI = 0.0016 is recommended based on the present study, but more data are necessary to accurately determine the threshold value. In addition, a blended model would be a further challenge to overcome because Moore et al. (2014) successfully used blended retrievals of Chl-*a* based on an optical water-type classification. As for MCI, Matsushita et al. (2015) indicated a relationship between MCI and Chl-*a* as mentioned in the "Methods" section.

Similarly to MCI, Matthews et al. (2012) proposed a comparison of reflectance peak height between 681

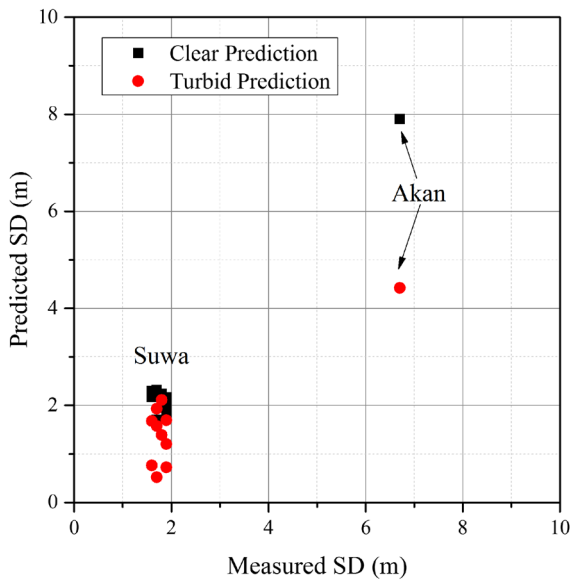

Fig. 8 Comparison of predicted SDs obtained using the clear and turbid water algorithms for Lakes Suwa and Akan, whose MCI values are in the range of 0.0001–0.0016

and 709 nm in order to separate oligotrophic/mesotrophic (peak at 681 nm) and eutrophic/hypertrophic waters (peak at 709 nm) using MERIS images. These peaks correspond to Chl-*a* fluorescence and particulate backscattering, respectively. Using this criterion, we obtained similar judgement results; peaks at 681 nm in Lakes Biwa, Shirakaba, Suwa, Ikeda, Unagi, Motosu, Shoji, and Sai, and peaks at 709 nm in Lakes Kasumigaura and Akan, and thus selection using the MCI is considered general and trustable.

Lastly, an exclusion of data for analysis is considered. A comparison between Cases 3 and 4 indicated that the meteorological conditions (i.e., waves and clouds), affected the SD prediction accuracy. We then investigated the statistical relationship between [L_{shade} divided by (E_{d}/π)] and the absolute value of ε_i for the dataset of Case 4 [i.e., (L_{shade} divided by (E_{d}/π)) <0.20], which was, however, judged to be insignificant ($R^2 = 0.078$, $P > 0.05$). In any case, a careful in situ measurement of reflectance spectra is needed.

Discrepancies between the measured and predicted SDs

Rather large discrepancies between the measured and predicted SDs were sometimes observed; especially, an underestimation, an overestimation, and scatters were revealed in Lake Kasumigaura (Fig. 6e), Lakes Sai and Shoji (Fig. 6d), and Lake Biwa (Fig. 6d), respectively. The IOP-retrieving algorithm for turbid waters was developed using the data taken in Lake Kasumigaura, and high accuracy was confirmed (Yang et al., 2013). Because the bias of the retrieving algorithm in visible wavelengths was particularly small, other factors would make an underestimation. When applying the method for the discrimination of cyano-dominant waters ($\mathrm{SICF}_{\mathrm{peak}} < 0$ and $\mathrm{SIPAF}_{\mathrm{peak}} > 0$; Matthews et al., 2012), the presence of cyano-dominance was detected in most of the reflectance spectra in Lake Kasumigaura except for an observation in March. A dominance of cyanobacteria has been observed in this lake from late spring to autumn (Fukushima & Arai, 2015), resulting in horizontally and vertically inhomogeneous patchy distributions of algae. Thus, such an accumulation (i.e., surface scum and patches of cyanobacteria), could probably affect the observation of SD, but the details and the effects on both SD observation and prediction should be investigated. In addition, the prediction scheme for the diffuse attenuation coefficient K_{d} [Eq. (5)] should be reexamined by other schemes for turbid waters (e.g., Yang et al., 2014).

In Lake Biwa, scatters were often observed for noisy reflectance spectra (7 August 2009; Fig. 2b). Noisy spectra were also obtained in Lakes Ikeda and Unagi (Fig. 2d), but good agreement between the measured and predicted SDs was observed. It thus seems unlikely that scatters are attributable to noisy reflectance spectra. In the case of Lakes Shoji and Sai, a relatively large overestimation was obtained. In these lakes, non-uniform vertical distributions of OASs are expected. Odermatt et al. (2012) indicated the importance of the vertical distribution of various parameters in a stratified lake to evaluate the MERIS observations of phytoplankton blooms. Phytoplankton blooms occur in different stratification layers, allowing the assessment of their influence on remote-sensing estimates. Such an influence should be investigated by both modeling and in situ measurements.

Conclusion

In the present study, we constructed a semi-analytical algorithm for estimating SD value using a remote-sensing reflectance spectrum. We compared the predicted SD values with the observed values in 10 Japanese lakes with a wide variety of turbidity. A fairly good agreement between the predicted and observed values was obtained indicating the usefulness of this prediction scheme. Our prediction scheme is almost analytical and therefore applicable to any lake in the world. In this context, our scheme promises to be one of the universal algorithms for SD prediction. However, further investigations are required on the relationships between Γ and SDs, blending algorithm, the influence of algal patchy distribution and/or a vertically non-uniform distribution of OASs on SD observation and prediction, the use of space-born data and more in order to improve the algorithm and its application.

Acknowledgments This research was supported in part by Grants-in Aid for Scientific Research from the Ministry of Education, Culture, Sport, Science and Technology (MEXT), Japan (Nos. 23404015 and 25420555), the Global Environment Research Fund (S9-4) of the Ministry of Environment, Japan, and the River Fund (27-1271-001) in charge of The River

Foundation, Japan. We express our appreciation to two anonymous reviewers for constructive criticisms on an earlier version of the manuscript.

References

Alparslan, E., C. Aydöner, V. Tufekci & H. Tüfekci, 2007. Water quality assessment at Ömerli Dam using remote sensing techniques. Environmental Monitoring and Assessment 135: 391–398.

Binding, C. E., J. H. Jerome, R. P. Bukata & W. G. Booty, 2007. Trends in water clarity of the lower Great Lakes from remotely sensed aquatic color. Journal of Great Lakes Research 33: 828–841.

Bowers, D. G., G. E. L. Harker, P. S. D. Smith & P. Tett, 2000. Optical properties of a region of freshwater influence (the Clyde Sea). Estuarine Coastal and Shelf Science 50: 717–726.

Chen, Z., F. E. Muller-Karger & C. Hu, 2007. Remote sensing of water clarity in Tampa Bay. Remote Sensing of Environment 109: 249–259.

Chipman, J. W., T. M. Lilles, J. E. Schmaltz, J. E. Leale & M. J. Nordheim, 2004. Mapping lake water clarity with Landsat images in Wisconsin, USA. Canadian Journal of Remote Sensing 30: 1–7.

Davies-Colley, R. J., 1988. Measuring water clarity with a black disk. Limnology and Oceanography 33: 616–623.

Doerffer, R. & H. Schiller, 2007. The MERIS case 2 water algorithm. International Journal of Remote Sensing 28: 517–535.

Doron, M., M. Babin, O. Hembise, A. Mangin & P. Garnesson, 2011. Ocean transparency from space: validation of algorithms using MERIS, MODIS and Sea WiFS data. Remote Sensing of Environment 115: 2986–3001.

Fukushima, T. & H. Arai, 2015. Regime shifts observed in Lake Kasumigaura, a large shallow lake in Japan: analysis of a 40-year limnological record. Lakes and Reservoirs: Research and Management 20: 54–68.

Giardino, C., M. Pepe, P. A. Brivio, P. Ghezzi & E. Zilioli, 2001. Detecting chlorophyll, Secchi disk depth and surface temperature in a sub-alpine lake using Landsat imagery. The Science of the Total Environment 268: 19–29.

Giardino, C., M. Bresciani, P. Villa & A. Martinelli, 2010. Application of remote sensing in water resource management: the case study of Lake Trasimeno, Italy. Water Resources Management 24: 3885–3899.

Gower, J., S. King, G. Borstad & L. Brown, 2005. Detection of intense plankton blooms using the 709 nm band of the MERIS imaging spectrometer. International Journal of Remote Sensing 26: 2005–2012.

Ha, J. Y., T. Hanazato, K. H. Chang, K. S. Jeong & D. K. Kim, 2015. Assessment of the lake biomanipulation mediated by piscivorous rainbow trout and herbivorous daphnids using a self-organizing map: a case study in Lake Shirakaba, Japan. Ecological Informatics 29: 182–191.

Hale, G. M. & M. R. Querry, 1973. Optical-constants of water in 200-nm to 200-micrometer wavelength region. Applied Optics 12: 555–563.

Härmä, P., J. Vepsäläinen, T. Hannonen, T. Pyhälahti, J. Kämäri, K. Kallio, K. Eloheimo & S. Koponen, 2001. Detection of water quality using simulated satellite data and semi-empirical algorithms in Finland. Science of the Total Environment 268: 107–121.

Hellweger, F. L., P. Schlosser, U. Lall & J. K. Weissel, 2004. Use of satellite imagery for water quality studies in New York Harbor. Estuarine, Coastal and Shelf Science 61: 437–448.

Hicks, B. J., G. A. Stichbury, L. K. Brabyn, M. G. Allan & S. Ashraf, 2013. Hindcasting water clarity from Landsat satellite images of unmonitored shallow lakes in the Waikato region, New Zealand. Environmental Monitoring and Assessment 185: 7245–7726.

Hoge, F. E. & P. E. Lyon, 1996. Satellite retrieval of inherent optical properties by linear matrix inversion of oceanic radiance models: an analysis of model and radiance measurement errors. Journal of Geophysical Research Oceans 101(C7): 16631–16648.

Holmes, R. W., 1970. Secchi disc in turbid coastal waters. Limnology and Oceanography 15: 688–694.

Japan Meteorological Agency, 2015. Past Meteorological Data [available on internet at http://www.data.jma.go.jp/obd/stats/etrn/]. Cited 14 October 2015.

Kabbara, N., J. Benkhelil, M. Awad & V. Barale, 2008. Monitoring water quality in the coastal area of Tripoli (Lebanon) using high-resolution satellite data. ISPRS Journal of Photogrammetry and Remote Sensing 63: 488–495.

Kirk, J. T. O., 1984. Dependence of relationship between inherent and apparent optical-properties of water on solar altitude. Limnology and Oceanography 29: 350–356.

Kloiber, S. M., P. L. Brezonik & M. E. Bauer, 2002. Application of Landsat imagery to regional-scale assessments of lake clarity. Water Research 36: 4330–4340.

Koponen, S., J. Pulliainen, K. Kallio & M. Hallikainen, 2002. Lake water quality classification with airborne hyperspectral spectrometer and simulated MERIS data. Remote Sensing of Environment 79: 51–59.

Kratzer, S., B. Haekansson & C. Sahlin, 2003. Assessing Secchi and photic zone depth in the Baltic Sea from satellite data. Ambio 32(8): 577–585.

Kratzer, S., C. Brockmann & G. Moore, 2008. Using MERIS full resolution data to monitor coastal waters – a case study from Himmerfjarden, a fjord-like bay in the northwestern Baltic Sea. Remote Sensing of Environment 112: 2284–2300.

Larson, G. L., R. Collier & M. W. Buktenica, 2007. Long-term limnological research and monitoring at Crater Lake, Oregon. Hydrobiologia 574: 1–11.

Lathrop, R. G., T. M. Lilles & B. S. Yandell, 1991. Testing the utility of simple multi-date Thematic Mapper calibration algorithms for monitoring turbid inland waters. International Journal of Remote Sensing 12: 2045–2063.

Lee, Z. P., K. L. Carder, R. G. Steward, T. G. Peacock, C. O. Davis & J. S. Patch, 1998. An empirical algorithm for light absorption by ocean water based on color. Journal of Geophysical Research Oceans 103(C12): 27967–27978.

Lee, Z. P., K. L. Carder & R. A. Arnone, 2002. Deriving inherent optical properties from water color: a multiband quasi-analytical algorithm for optically deep waters. Applied Optics 41(27): 5755–5772.

Lee, Z. P., K. P. Du & R. Arnone, 2005. A model for the diffuse attenuation coefficient of downwelling irradiance. Journal of Geophysical Research Oceans 110(C02): 016.

Lee, Z. P., A. Weidemann, J. Kindle, R. Arnone, K. L. Carder & C. Davis, 2007. Euphotic zone depth: its derivation and implication to ocean-color remote sensing. Journal of Geophysical Research Oceans 112(C3): 009.

Lee Z. P., B. Lubac, J. Werdell & R. Arnone, 2009. An update of the quasi-analytical algorithm (QAA_v5) [available on internet at http://www.ioccg.org/groups/Software_OCA/QAA_v5.pdf]. Cited 20 October 2014.

Mancino, G., A. Nole, V. Urbano, M. Amato & A. Ferrara, 2009. Assessing water quality by remote sensing in small lakes: the case study of Monticchio lakes in southern Italy. iForest: Biogeoscience and Forestry 2: 154–161.

Matsushita, B., W. Yang, G. Yu, Y. Oyama, K. Yoshimura & T. Fukushima, 2015. A hybrid algorithm for estimating the chlorophyll-*a* concentration across different trophic states in Asian inland waters. ISPRS Journal of Photogrammetry and Remote Sensing 102: 28–37.

Matthews, M. W., S. Bernard & L. Robertson, 2012. An algorithm for detecting trophic status (chlorophyll-*a*), cyanobacterial-dominance, surface scums and floating vegetation in inland and coastal waters. Remote Sensing of Environment 124: 637–652.

Mobley, C. D., 1999. Estimation of the remote-sensing reflectance from above-surface measurements. Applied Optics 38: 7442–7455.

Mobley, C. D., B. Gentili, H. R. Gordon, Z. H. Jin, G. W. Kattawar, A. Morel, P. Reinersman, K. Stamnes & R. H. Stavn, 1993. Comparison of numerical-models for computing underwater light fields. Applied Optics 32: 7484–7504.

Moore, T. S., M. D. Dowell, S. Bradt & A. R. Verdu, 2014. An optical water type framework for selecting and blending retrievals from bio-optical algorithms in lakes and coastal waters. Remote Sensing of Environment 143: 97–111.

Morel, A., 1974. Optical properties of pure sea water. In Optical Aspects of Oceanography. Academic, London.

Nakagawa, K., 2015. Calculation of zenith angle [available on internet at http://www.es.ris.ac.jp/~nakagawa/met_cal/solar.html]. Cited at 15 February 2015.

Nelson, S. A., P. A. Soranno, K. S. Cheruvelil, S. A. Batzli & D. L. Skole, 2003. Regional assessment of lake water clarity using satellite remote sensing. Journal of Limnology 62(Suppl. 1): 27–32.

Odermatt, D., F. Pomati, J. Pitarch, J. Carpenter, M. Kawka, M. Schaepman & A. Wueest, 2012. MERIS observations of phytoplankton blooms in a stratified eutrophic lake. Remote Sensing of Environment 126: 232–239.

Olmanson, L. G., M. E. Bauer & P. L. Brezonik, 2008. A 20-year Landsat water clarity census of Minnesota's 10000 lakes. Remote Sensing of Environment 112: 4086–4097.

Olmanson, L. G., P. L. Brezonik & M. E. Bauer, 2014. Geospatial and temporal analysis of a 20-year record of Landsat-based water clarity in Minnesota's 10,000 lakes. Journal of the American Water Resources Association 50(3): 748–761.

Pope, R. M. & E. S. Fry, 1997. Absorption spectrum (380–700 nm) of pure water. 2. Integrating cavity measurements. Applied Optics 36: 8710–8723.

Preisendorfer, R. W., 1986. Secchi disc science – visual optics of natural-waters. Limnology and Oceanography 31: 909–926.

Reference Solar Spectral Irradiance – ASTM G-173 [available on internet at http://rredc.nrel.gov/solar/spectra/am1.5/ASTMG173/ASTMG173.html]. Cited 15 February 2015.

Roesler, C. S. & M. J. Perry, 1995. In-situ phytoplankton absorption, fluorescence emission, and particulate backscattering spectra determined from reflectance. Journal of Geophysical Research Oceans 100(C7): 13279–13294.

Sass, G. Z., I. F. Creed, S. E. Bayley & K. J. Devito, 2007. Understanding variation in trophic status of lakes on the Boreal Plain: a 20 year retrospective using Landsat TM imagery. Remote Sensing of Environment 109: 127–141.

Sawaya, K. E., L. G. Olmanson, N. J. Heinert, P. L. Brezonik & M. E. Bauer, 2003. Extending satellite remote sensing to local scales: land and water resource monitoring using high-resolution imagery. Remote Sensing of Environment 88: 144–156.

SCOR UNESCO, 1966. Determination of photosynthetic pigment in seawater. Monographs on Oceanographic Methodology. UNESCO, Paris.

Takami, S., 2011. Light measurement in ecological studies. Climate in Biosphere 11: A1–A7 (in Japanese).

Terrel, M. M., T. Fukushima, B. Matsushita, K. Yoshimura & A. Imai, 2012. Long-term light environment variability in Lake Biwa and Lake Kasumigaura, Japan: modeling approach. Limnology 13(2): 237–252.

Tyler, J. E., 1968. The Secchi disc. Limnology and Oceanography 13: 1–6.

Wu, G., J. Leeuw, A. K. Skidmore, H. T. Prins & Y. Liu, 2008. Comparison of MODIS and Landsat TM5 images for mapping tempo-spatial dynamics of Secchi disk depths in Poyang Lake National Nature Reserve, China. International Journal of Remote Sensing 29: 2183–2198.

Yang, W., B. Matsushita, J. Chen, K. Yoshimura & T. Fukushima, 2013. Retrieval of inherent optical properties for turbid inland waters from remote-sensing reflectance. IEEE Transactions on Geoscience and Remote Sensing 51: 3761–3773.

Yang, W., B. Matsushita, J. Chen, K. Yoshimura & T. Fukushima, 2014. Application of a semianalytical algorithm to remotely estimate diffuse attenuation coefficient in turbid inland waters. IEEE Geoscience and Remote Sensing Letters 11: 1046–1050.